First Measurement Campaign using the Target Detector and a Full Readout Chain for the Neutrinos Angra Project

Anjos, J. C. [a], Azzi, G. [a], Cerqueira, A. S. [b], Chimenti, P. [c], Costa, J. A. [b], Dornelas, T. I. [b*], Farias, P. C. M. A. [d], Guedes, G. P. [e], Gonzalez, L. F. G. [f], Kemp, E. [f], Lima Jr, H. P. [a*], Machado, R. [a], Nóbrega, R. A. [b*], Pepe, I. M. [d], Ribeiro, D. B. S. [d], Simas Filho, E. F. [d], Valdiviesso, G. A. [g], Wagner, S. [a],

(a) Centro Brasileiro de Pesquisas Físicas, CBPF, Rio de Janeiro-RJ, Brazil
(b) Universidade Federal de Juiz de Fora, UFJF, Juiz de Fora-MG, Brazil
(c) Universidade Federal do ABC, UFABC, Santo André-SP, Brazil
(d) Universidade Federal da Bahia, UFBA, Salvador-BA, Brazil
(e) Universidade Estadual de Feira de Santa, UEFS, Feira de Santa-BA, Brazil
(f) Universidade Estadual de Campinas, UNICAMP, Campinas-SP, Brazil
(g) Universidade Federal de Alfenas, UNIFAL-MG, Poços de Caldas-MG, Brazil

Abstract

In this document we describe the setup and the achieved results of the first measurement campaign applying the full chain of the readout system on the Neutrinos-Angra target detector, which was equipped with 16 8-inches PMTs located on its bottom side. The readout system made use of two front-end cards and two acquisition modules in order to read and digitize all the PMT output signals. This campaign was divided in two parts: the first one to test and to debug the readout system and the second one to perform an acquisition run based on cosmic rays detection. Two scintillator pads have been used in coincidence to trigger the events. The measurement campaign resulting achievements were: a successful test of the target detector and the validation of the Neutrinos Angra readout system.

*Corresponding authors, e-mails: tony.dornelas@engenharia.ufjf.br, hlima@cbpf.br, rafael.nobrega@ufjf.edu.br

1 Introduction

The Neutrinos-Angra target detector has been recently assembled with its 16 bottom PMTs. To equip the detector, the front-end [1] [2] and the acquisition [3] modules have been put together with the objective to assess for the first time the target detector and to validate a full readout chain of the Neutrinos-Angra Project.

2 Setup description

2.1 The Target Detector

As mentioned before, in the context of this document the target detector was partially mounted: only the bottom PMTs were installed. Figures 1 and 2 shows four PMTs ready to be inserted into the detector and the 16 PMTs fully installed on the bottom of the detector, respectively. The right picture of Figure 2 maps the position of each PMT based on their serial numbers. It is also possible to see that the inner walls of the detector were all covered with the tyvek material.

Figure 1: Four PMTs on their support before installing them inside the target detector.

Figure 2: PMT devices installed on the bottom of the target detector (left) and its corresponding mapping using the PMT devices' serial numbers (use as reference the triangle located on the corner) (right)

.

After covering the inner walls with Tyvek sheets and PMT installation, the detector was flooded with 1370 liters of filtered water. A small volume was left empty in order to avoid the contact between the used endcap and the water itself. The target detector was then covered by an endcap and a black tarp to seal and to protect the detector from external light. The PMT cables (signal and HV) were

then routed to the control room located just few meters from the detector. Figure 3 shows the detector completed sealed, after PMT installation.

Figure 3: Picture of the detector assembled, filled with water and sealed.

2.2 The High-Voltage Power Supply

The PMTs have been characterized by Hamamatsu to operate with a gain of 10^7 and we are simply applying the provided high-voltage values for that gain. The CAEN SY4527 system was used as the power supply to all 16 installed PMTs. This system was controlled by a local computer also located in the CBPF control room. Table 1 shows the connection mapping between the CAEN module channels (Ch) and the PMTs with their respective supply values (HV).

Table 1: High-Voltage system connections.

Ch	PMT	HV (V)	Ch	PMT	HV (V)	Ch	PMT	HV (V)	Ch	PMT	HV (V)
00	2850	1510	04	2806	1550	08	2759	1660	12	2778	1370
01	2801	1570	05	2855	1470	09	2784	1480	13	2790	1430
02	2794	1400	06	2836	1570	10	2847	1540	14	2770	1430
03	2786	1430	07	2787	1420	11	2789	1430	15	2857	1530

A high-voltage NIM module (N1470) was used to power supply the scintillator pads applied for the trigger system. Both were supplied with a voltage value of 1450 V.

2.3 The Readout System

A scheme of the applied readout system is presented in Figure 4. The 16 PMTs signal cables were connected to the input of the front-end cards, which have been configured to operate with a lower gain in relation to the original specifications. This change was needed to make it possible to detect cosmic rays instead of the antineutrino decay particles. The front-end output signals were sent to the NDAQ modules, where the signals are finally digitalized and sent to a local computer via a VME controller by means of Ethernet protocol. Two scintillator pads (active area dimensions: 14cm x 14cm, with

1 cm of thickness) were positioned just above the detector to trigger cosmic events. Their signals were sent to a discriminator which was configured to work with the minimum possible threshold value of -25 mV and a logic port configured to provide coincidence between the scintillators. The resulting signal was sent to the NDAQ modules trigger inputs making use of a fanout NIM module. The NDAQ modules have been configured to digitize 100 samples (800ns) of the input signals each time it receives a trigger pulse (20 samples before and 80 samples after the trigger rising edge).

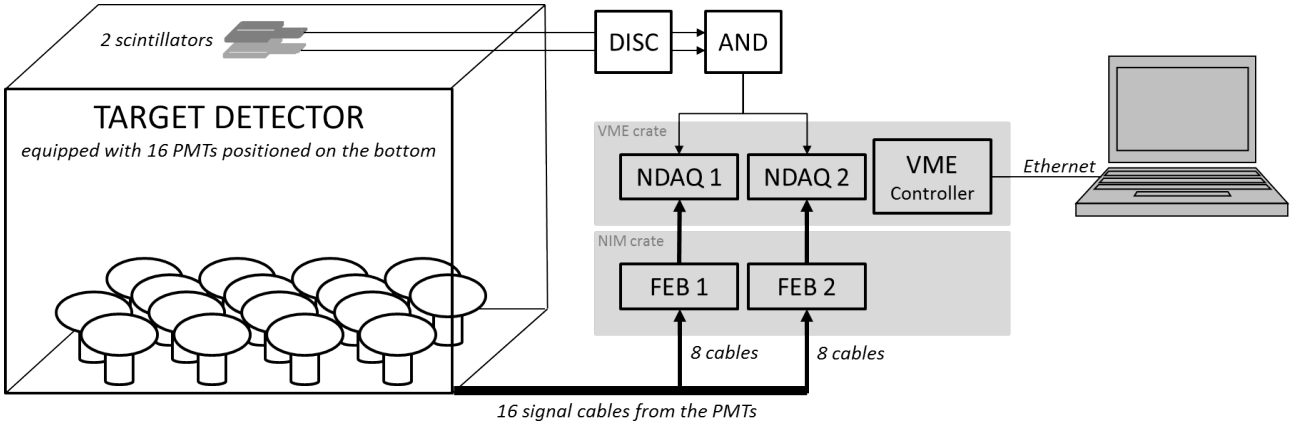

Figure 4: Scheme of the applied readout system to acquire cosmic events.

Two typical signals as produced by the readout system are presented in Figure 5.

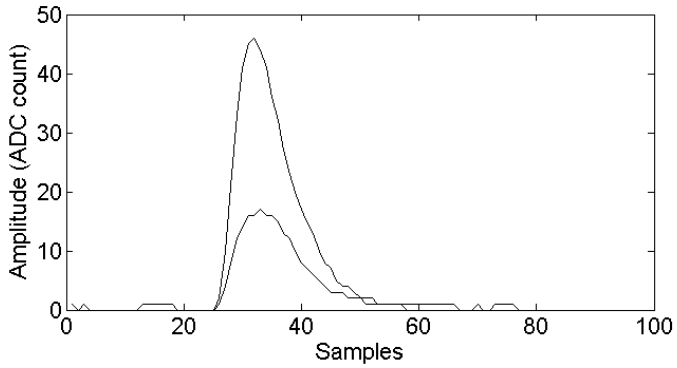

Figure 5: Example of two typical signals produced by the readout system.

2.4 Detecting, identifying and solving the readout setup faults

In the first set of measurements some unexpected problems were found with the front-end and the NDAQ modules. As an example, Figure 6 shows two types of degraded signals, one labeled as Class A and another as Class B. The former saturates at about 800 mV and the latter at a region around 400 mV of peak amplitude. Both have their shape deformed, even when the front-end does not saturate, and an unexpected effect of undershoot in both signal classes are present.

Figure 7 shows the peak amplitude versus the amplitude sum of the samples for the 16 channels as acquired by the acquisition system. The first eight plots on the top are referred to the front-end board number 5, the 16 on the bottom are from the front-end board number 2. As it is possible to see, the A-Class and B-Class signals are visible end easily identifiable. The former saturates at about 400 ADC counts (800 mV) and the latter around 200 ADC counts (400 mV). The plots show that the area of the signal grows linearly with the peak amplitude up to a value where the peak amplitude saturates. At this moment, the peak amplitude is kept constant while the signal width continues to grow.

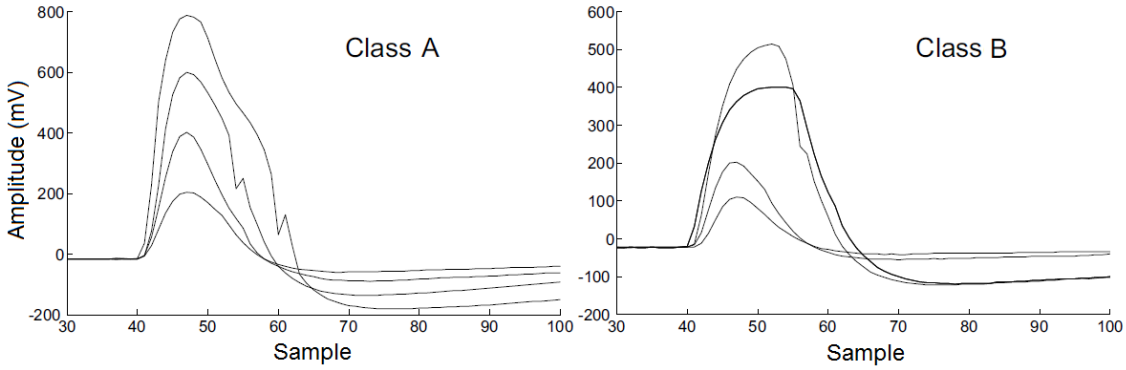

Figure 6: Example of corrupted acquired signals.

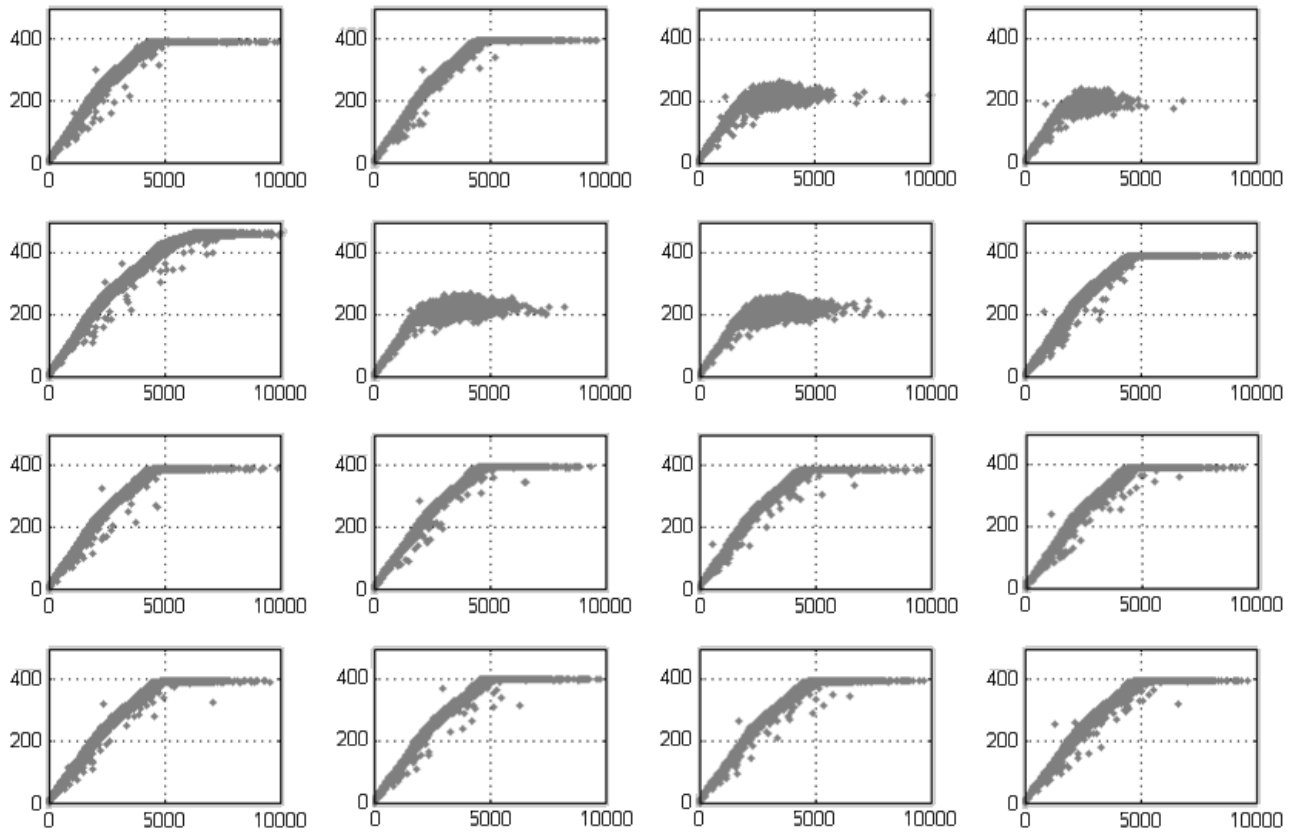

Figure 7: Peak amplitude versus amplitude sum of the samples, both in unit of ADC count.

It is important to notice that, considering the applied NDAQ version, 10 bits are used to convert the front-end signals within a dynamic range from -1V to 1V. The front-end circuit is expected to saturate only when its output signal reaches an amplitude value above 1.4 Volts. Therefore, those plots are expected to saturate at 512 ADC counts, before front-end saturation.

Going further and looking more carefully to the plots in Figure 7 it is possible to see that at about 250 ADC counts (vertical axis), there is a linearity break. Figure 8 shows the signal shape for different peak amplitudes. Notice that for peak amplitude values above 250 ADC counts, the signal shape begins to deform. For the peak amplitude value of 320 ADC counts, the deformation is strong and clear. This effect is visibly related to the linearity break mentioned before.

The results presented led us to consider that the installed front-end and NDAQ modules were not working as expected. The faults were identified and fully solved, as it will be shown in the next sections (2.4.1 and 2.4.2), and a new and successfully acquisition run was performed (section 3).

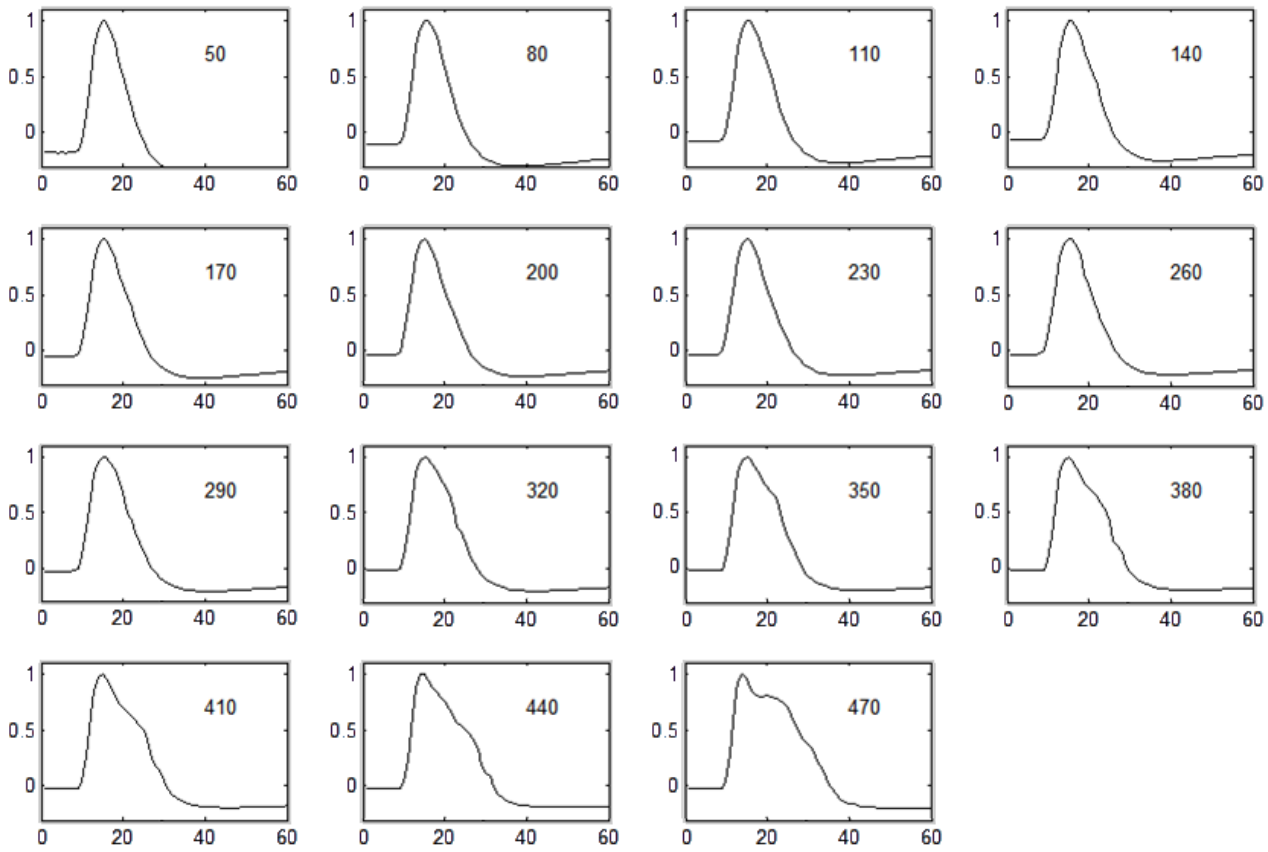

Figure 8: Normalized mean shape of the acquired signals for different peak amplitude values, going from 50 to 470 ADC counts as specified inside the internal area of each plot.

2.4.1 Identifying and solving the front-end faults

The front-end boards used to the first set of measurements were taken to the UFJF university to be tested in laboratory, where the following plots helped to identify the problems. Figure 9 shows the linearity curve for all the FE channels. As it can be seen, while the front-end number 2 presents a more stable behavior, the front-end number 5 presents two curve types, one loosing its linearity at about 1.4 Volts, which is expected, and another loosing it at about 0.5 Volts, showing that something is wrong with those latter channels.

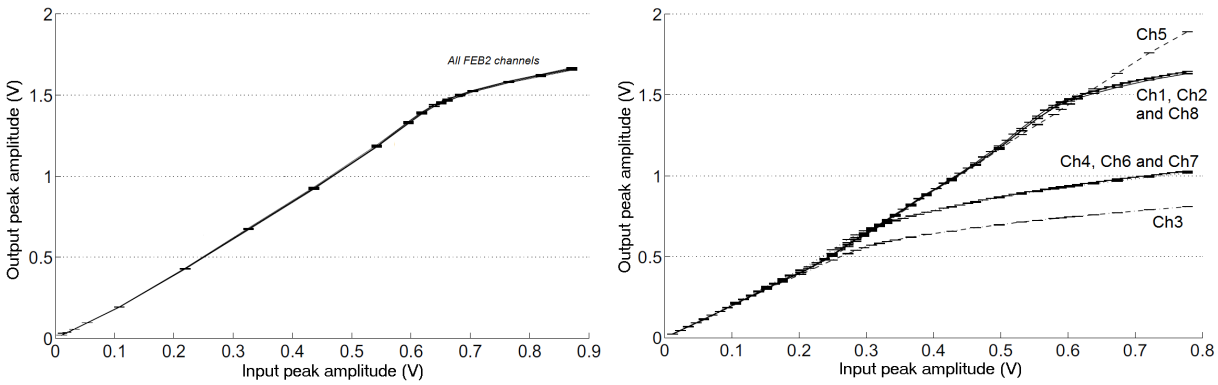

Figure 9: Linearity curves for the front-end boards 2 and 5, respectively.

An inspection on the front-end board components revealed that some of them were mistaken, presenting different values from the ones in the circuit design. The problems were fixed and two new front-end boards were sent to CBPF.

2.4.2 Identifying and solving the NDAQ faults

Three NDAQ modules were inspected, serial numbers 07, 15 and 20. The proposed test was based on the injection of Gaussian shaped signals into the NDAQ input ports using an arbitrary waveform generator. Signals with five different peak amplitude values were injected: 250 mV, 500 mV, 750 mV, 1000 mV and 1250 mV. The resulting curves (input peak amplitude versus output peak amplitude) are shown in Figure 10 where it is possible to note that two of the NDAQ modules presented nonlinear characteristics.

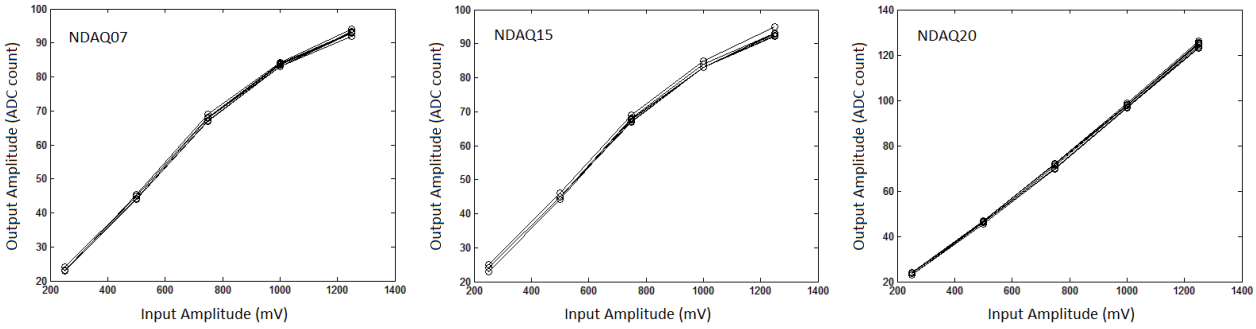

Figure 10: Linearity curves for the NDAQ modules 07, 15 and 20 obtained via signal injection using waveform generator.

A validation test on the shape of the signal as generated by the NDAQ modules was also carried out. Figures 11 and 12 show the results for the NDAQ15 and NDAQ20 modules. Note that the NDAQ15 module channels, other than being nonlinear, also deform the input signal; notice that this distortion is similar to the effect shown before in Figure 8.

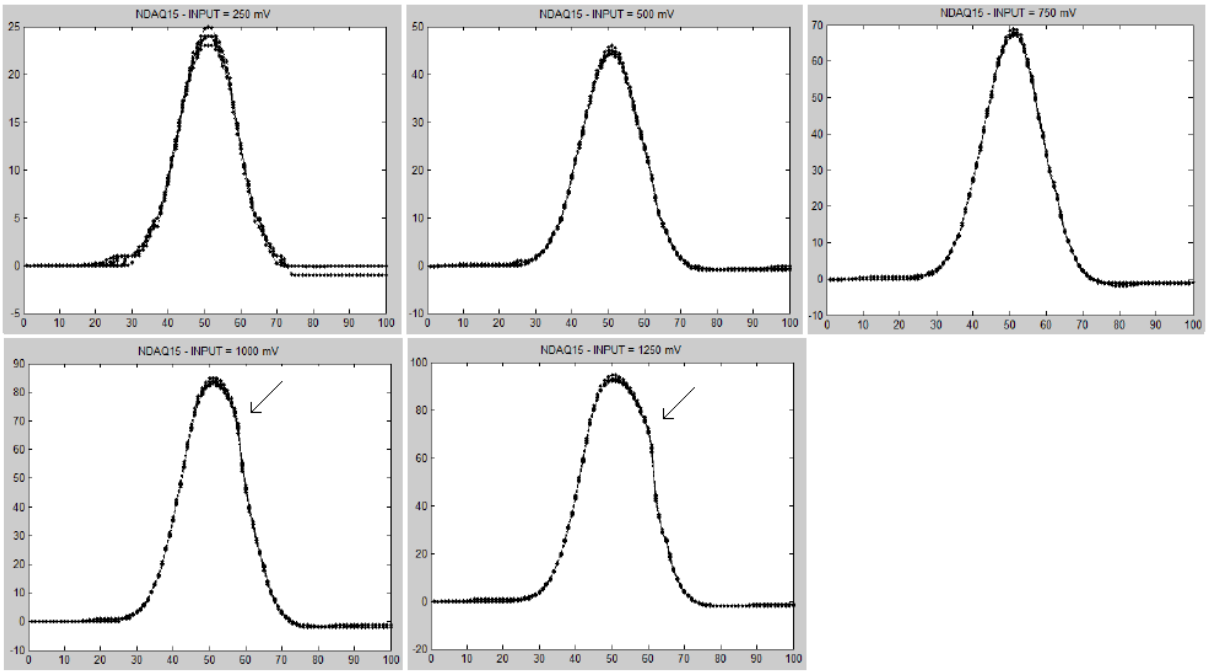

Figure 11: Shape of the signal after ADC conversion using the NDAQ 15.

Investigating the problem, it was realized that the NDAQ 20 module was the only one without the RF transformer connected right at the analog inputs. To fix the problem, all the RF transformers were removed from the NDAQs 07 and 15. After that it could be seen that the degradation in the ADC output counts vanished.

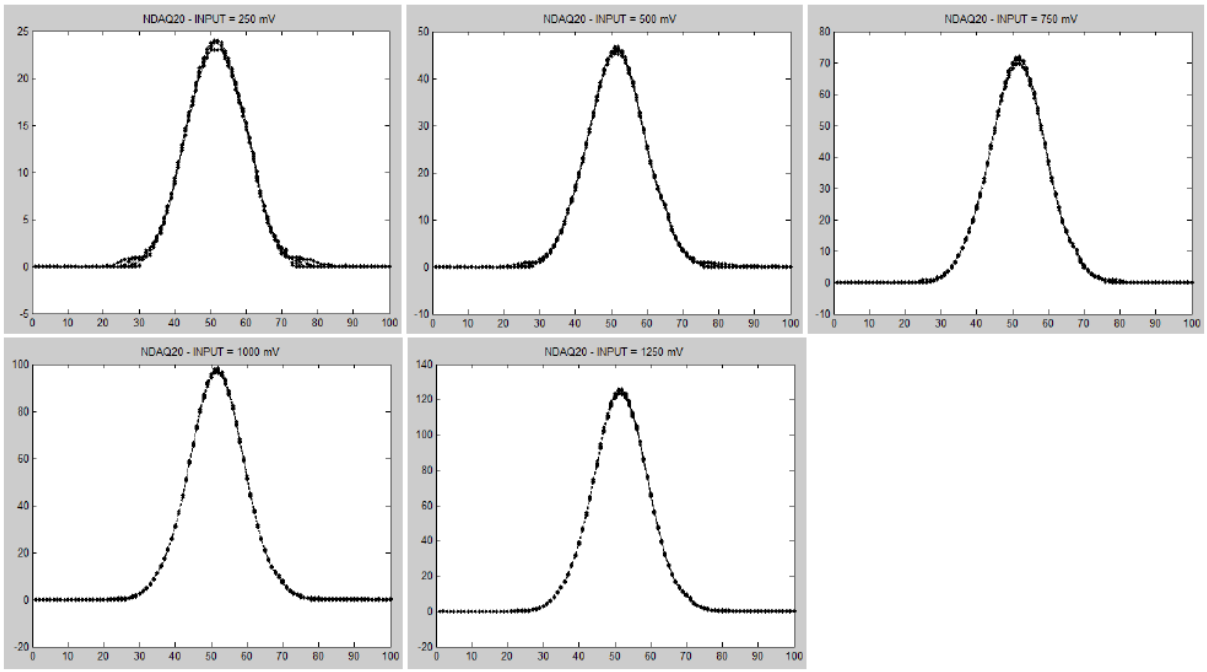

Figure 12: Shape of the signal after ADC conversion using the NDAQ 20.

3 Measurements based on cosmic rays acquisition

After fixing the problems above described, the front-end and NDAQ modules were re-calibrated and each single channel was checked individually. Subsequently, a new cosmic rays acquisition run has been carried out using as trigger the coincidence signals of the two scintillator pads on the top of the detector. It is important to notice that, for this new acquisition run, the front-end gain was reduced in order to acquire the cosmic rays high-amplitude-level produced signals while the NDAQ was configured to work with 8-bit ADC resolution within an interval between -1.250 and 1.250 Volts as it will be shown in the next subsections. Table 2 maps the signal connections between the readout devices.

Table 2: Readout system connections mapping.

NDAQ20	FEB02	PMT
01	08	2787
02	07	2836
03	06	2855
04	05	2806
05	04	2786
06	03	2794
07	02	2801
08	01	2850

NDAQ07	FEB04	PMT
01	08	2857
02	07	2770
03	06	2790
04	05	2778
05	04	2789
06	03	2847
07	02	2784
08	01	2759

3.1 The front-end and NDAQ calibrations

Front-end calibration: To work with a lower gain to avoid signal saturation caused by high amplitude PMT signals generated by cosmic rays, a voltage divider circuit was placed at the input of each front-end channel, using a resistor of 47 ohms in series and a resistance of 5 ohms in parallel, connected to ground, in a way to keep an impedance match of approximately 50 ohms as seen by the PMT output signal. Therefore, at the input of the front-end circuit, after the voltage divider circuit,

we have an amplitude reduction by a factor of 10.4 in relation to the PMT arriving signal. Using the front-end nominal gain of $24.69 \cdot 10^{-3}$ output peak amplitude per input charge [2], the new gain value to be used in the measurements presented in this section is $2.374 \cdot 10^{-3}$. which leads to the calibration curves presented in Figure 13, considering a PMT gain of 10^7. It should be taken into account that the front-end output signal saturates approximately at an amplitude value of 1.4 V.

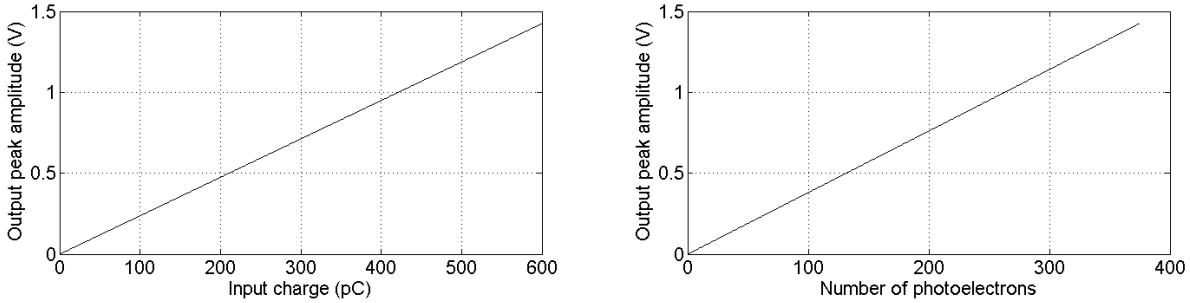

Figure 13: Front-end calibration curves.

NDAQ calibration: Figure 14 shows the calibration curves constructed by means of injecting signal with a waveform generator into the NDAQ07 and NDAQ20 modules. With those curves we can conclude that the NDAQ is working with a amplitude resolution which corresponds to and 8-bit ADC operating within a dynamic range from -1.25V to 1.25V, leading to a resolution of approximately 9.8 mV/ADC count, as expected.

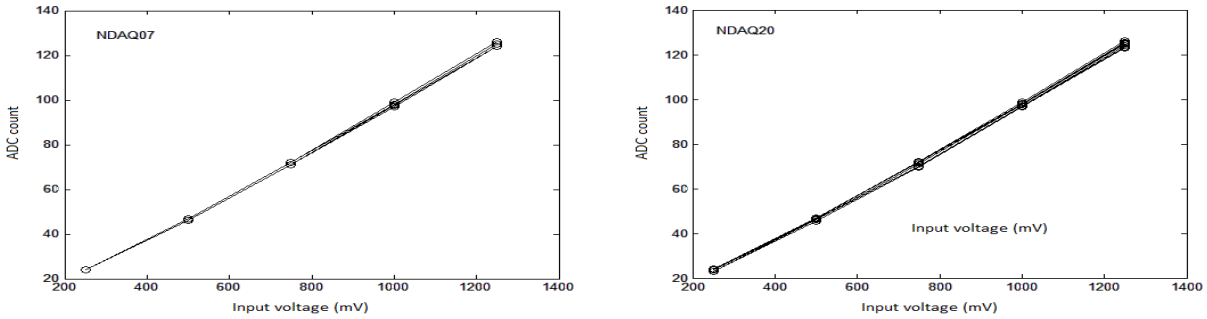

Figure 14: Calibration curves for the 16 channels corresponding to the NDAQs 07 (left) and 20 (right).

3.2 Channel-by-channel checking

After supplying power to all the PMT sensors, the signal of each individual channel was checked by performing an oscilloscope acquisition with the persistence option activated and programed to last 5 seconds. The results can be seen in Figures 15 and 16, for the front-end boards 2 and 4 respectively. If we compare the amplitude variation between the geometrically symmetric PMT devices (e.g. SD2850-SD2789, SD2836-SD2790, SD2806-SD2857, etc), it is possible to conclude that the configured PMT devices gains are not excessively discrepant among them.

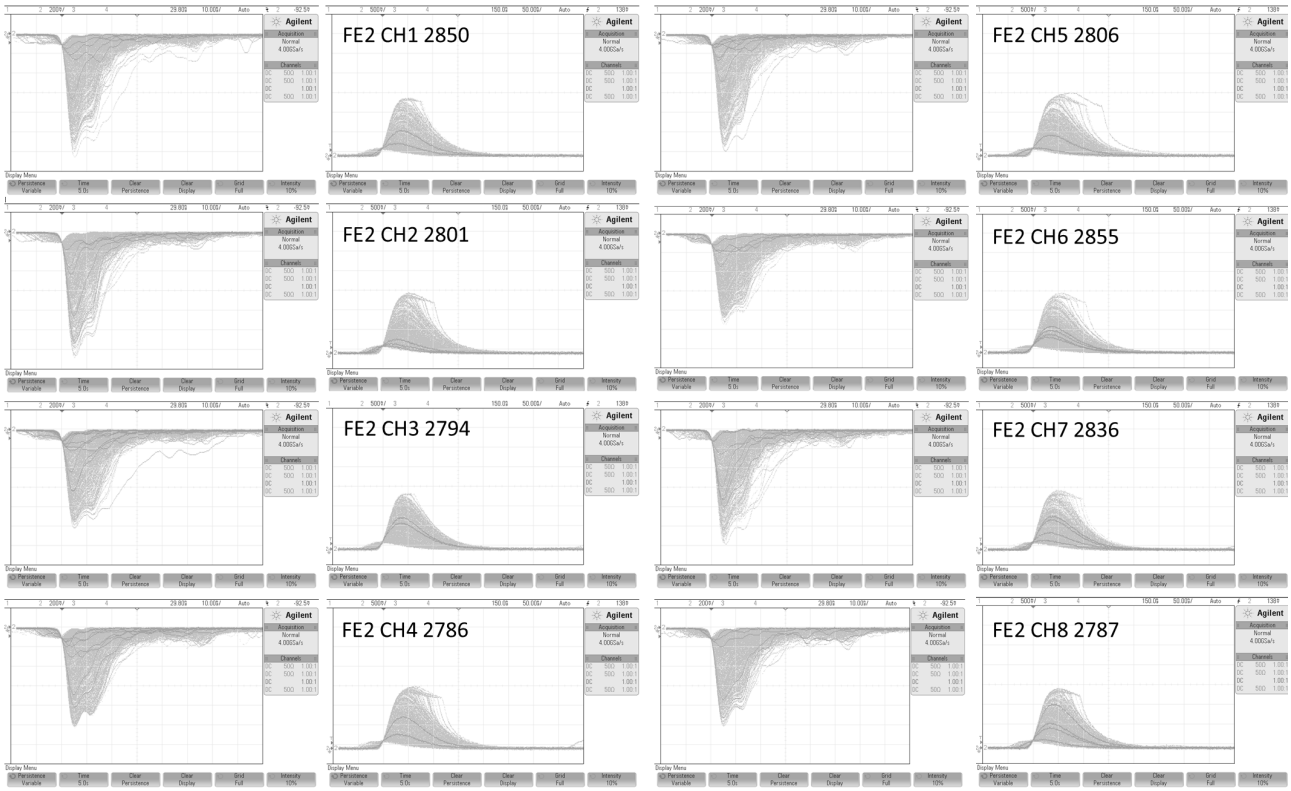

Figure 15: PMT and front-end signals for all the channels connected to the front-end board 2.

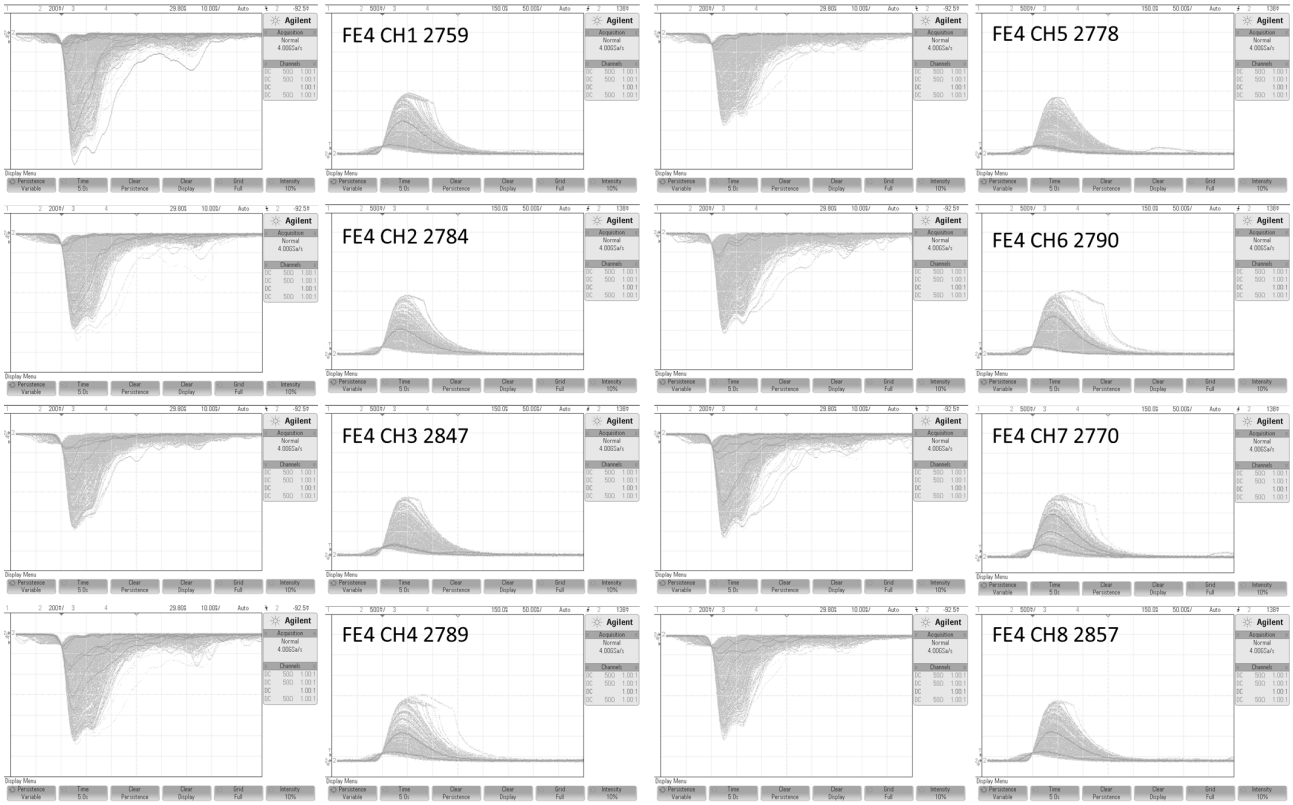

Figure 16: PMT and front-end signals for all the channels connected to the front-end board 4.

3.3 Results

After carefully checking all the system channels, a cosmic rays acquisition has been carried out, storing 10000 events in total. Figure 17 shows the distribution of coincidences between PMT sensors. As it can be seen, about 4000 events did not produce signal inside the detector. Those events might have been triggered by noise instead of cosmic particles. It is also possible to see that most of the events fired up all the 16 installed PMTs.

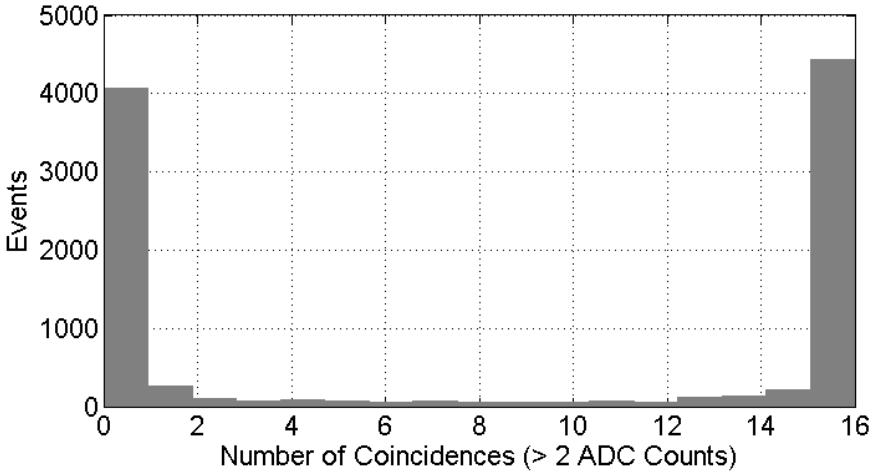

Figure 17: Distribution of the number of coincidences.

The listed figures show the results concerning each detector channel based on the acquired data:

- Figure 18: acquired time windows of the first 100 events;
- Figure 19: noise distribution in ADC count;
- Figure 20: peak amplitude versus sum of amplitudes;
- Figure 21: peak amplitude distribution in ADC counts;
- Figure 22: peak amplitude distribution in photoelectrons.

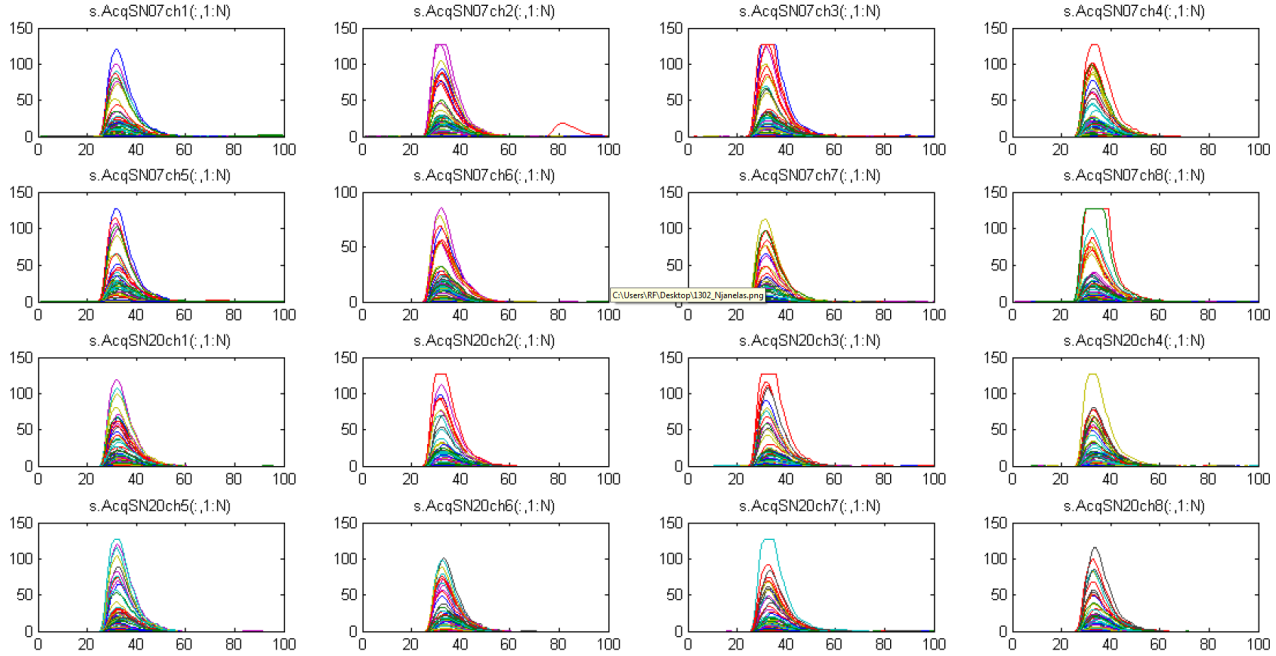

Figure 18: Acquired time windows of the first 100 events for all the PMT sensors: ADC count versus Sample.

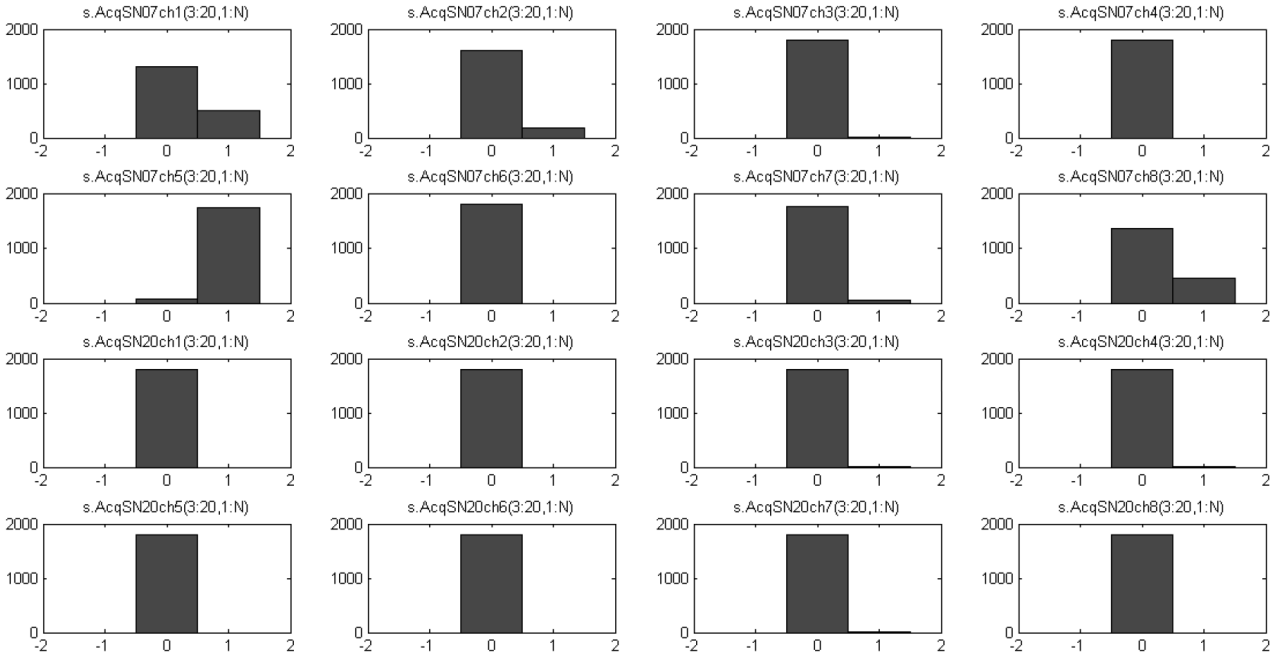

Figure 19: Noise distribution in ADC counts.

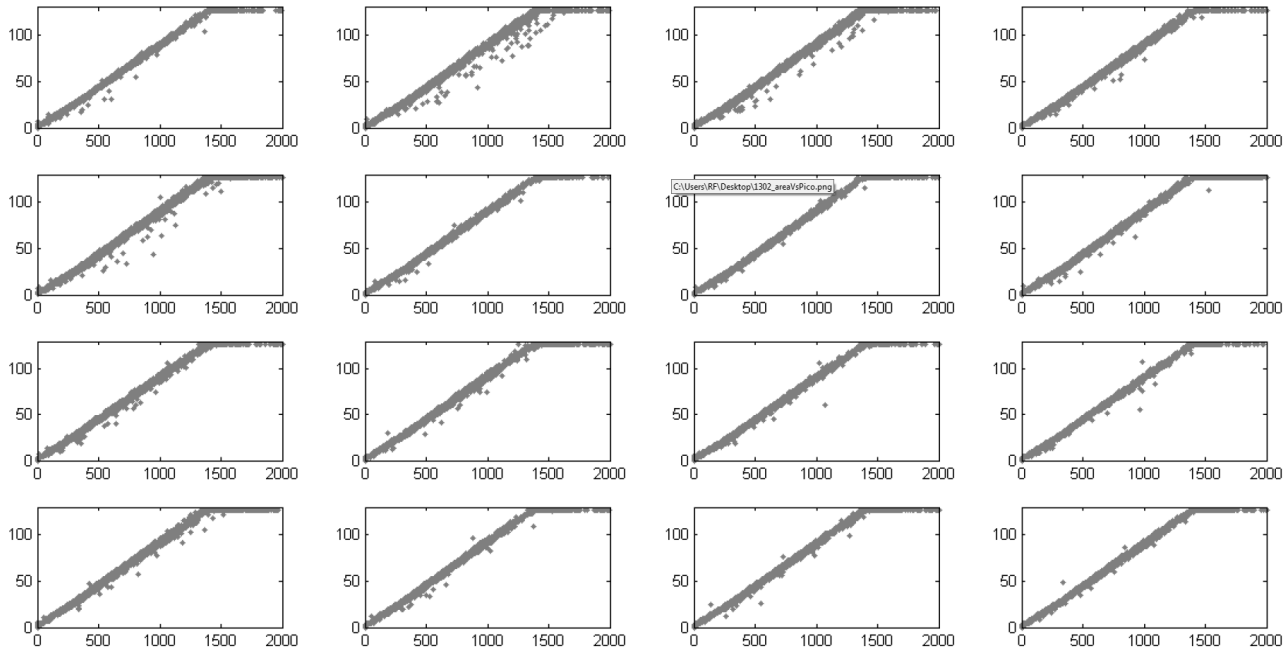

Figure 20: Peak amplitude versus Sum of the amplitudes for all the acquired channels in ADC count.

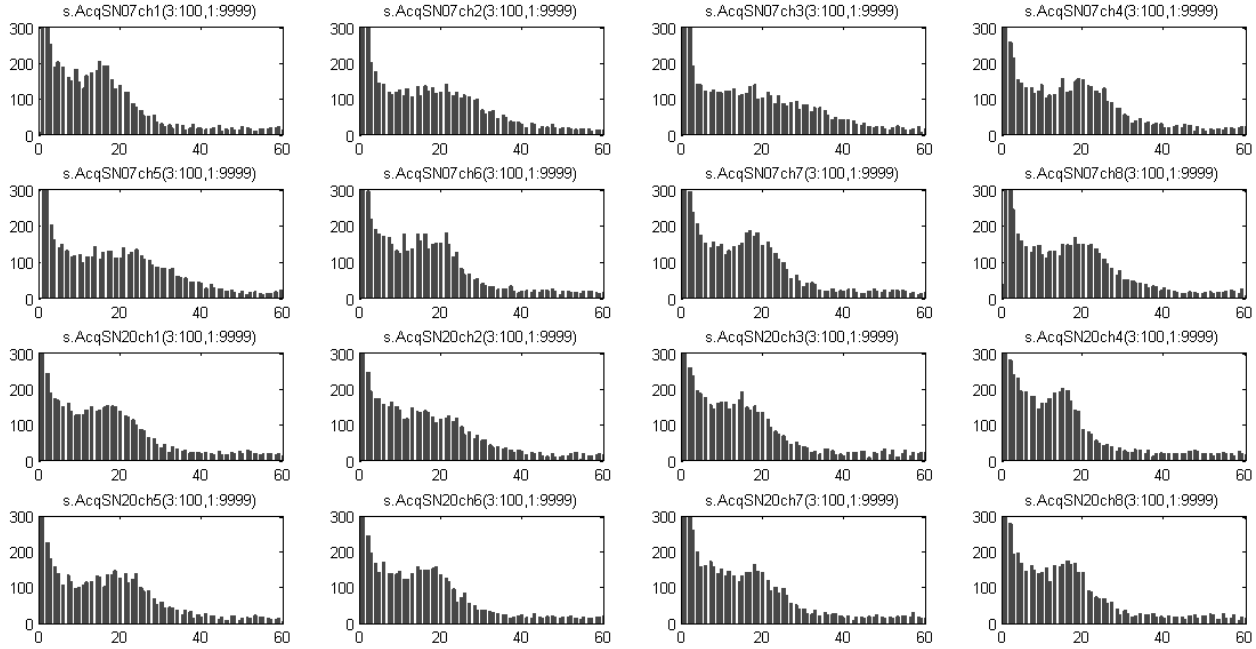

Figure 21: Peak amplitude distribution per PMT in ADC count.

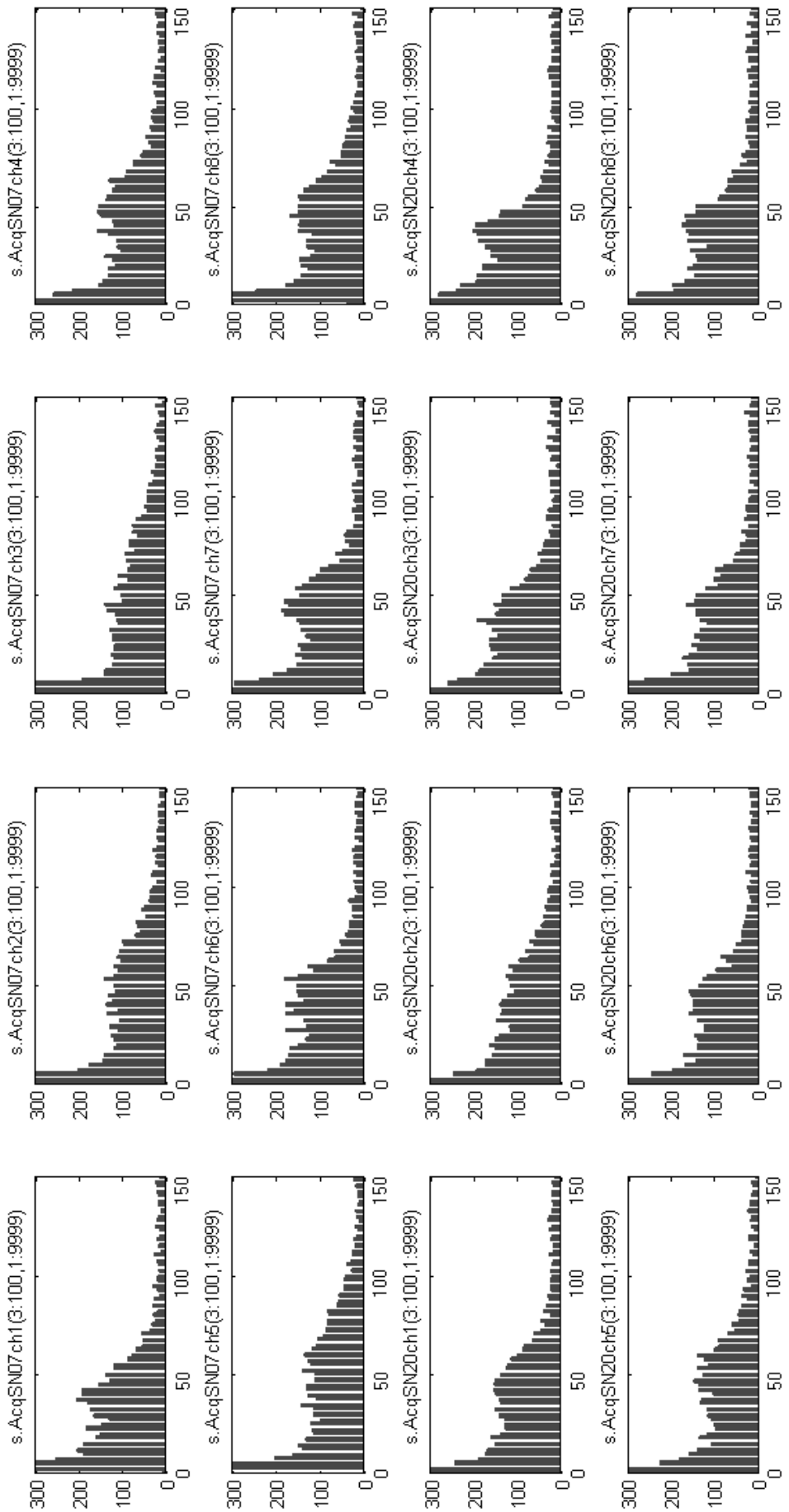

Figure 22: Photoelectrons distribution per PMT.

About 2% of the signals have entered into the NDAQ saturation region, which occurs at 127 ADC counts. Those saturated signals have been recovered by means of a χ^2-based fit algorithm using the mean shape of the front-end output signal as reference. Figure 23 shows examples of six recovered signals. This algorithm was used to estimate the peak value of the saturated signals. As it can be noticed, above a peak value of about 180 ADC counts, the signal shape is deformed, mainly on the falling edge, making the used algorithm less precise. Nevertheless, the number of signals with peak amplitude higher than 180 ADC counts is small, representing 0.4% of the total. Figure 24 shows the peak amplitude distribution for all the 16 PMT devices, after applying the fitting algorithm.

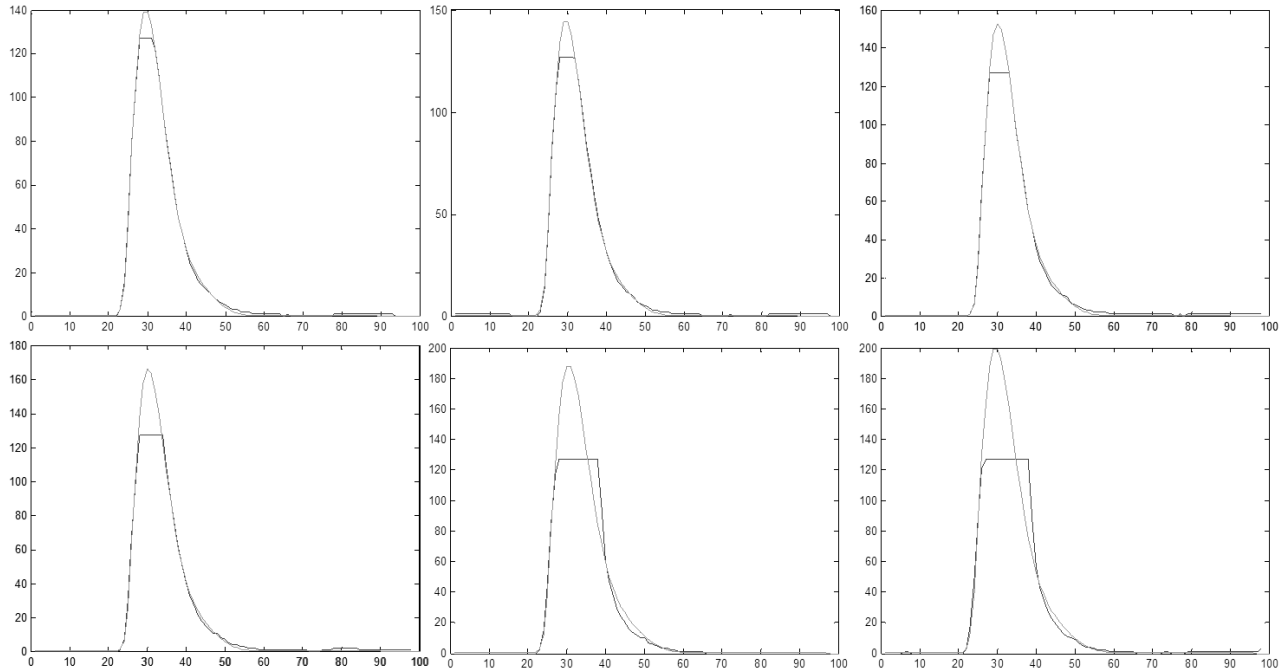

Figure 23: Saturated signals recovered by a χ^2-based fit algorithm (amplitude in ADC counts versus time in sample units).

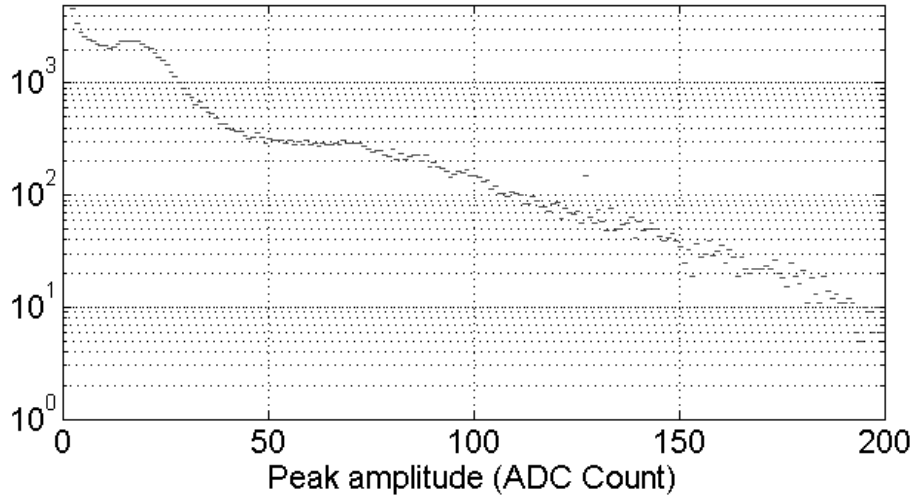

Figure 24: Peak amplitude distribution considering all the 16 PMT devices.

Figure 25 shows the distribution of the peak amplitude (top) and the number of photoelectrons (bottom) event-by-event sums considering all the PMT devices. The latter can be compared to the simulation results found here [4].

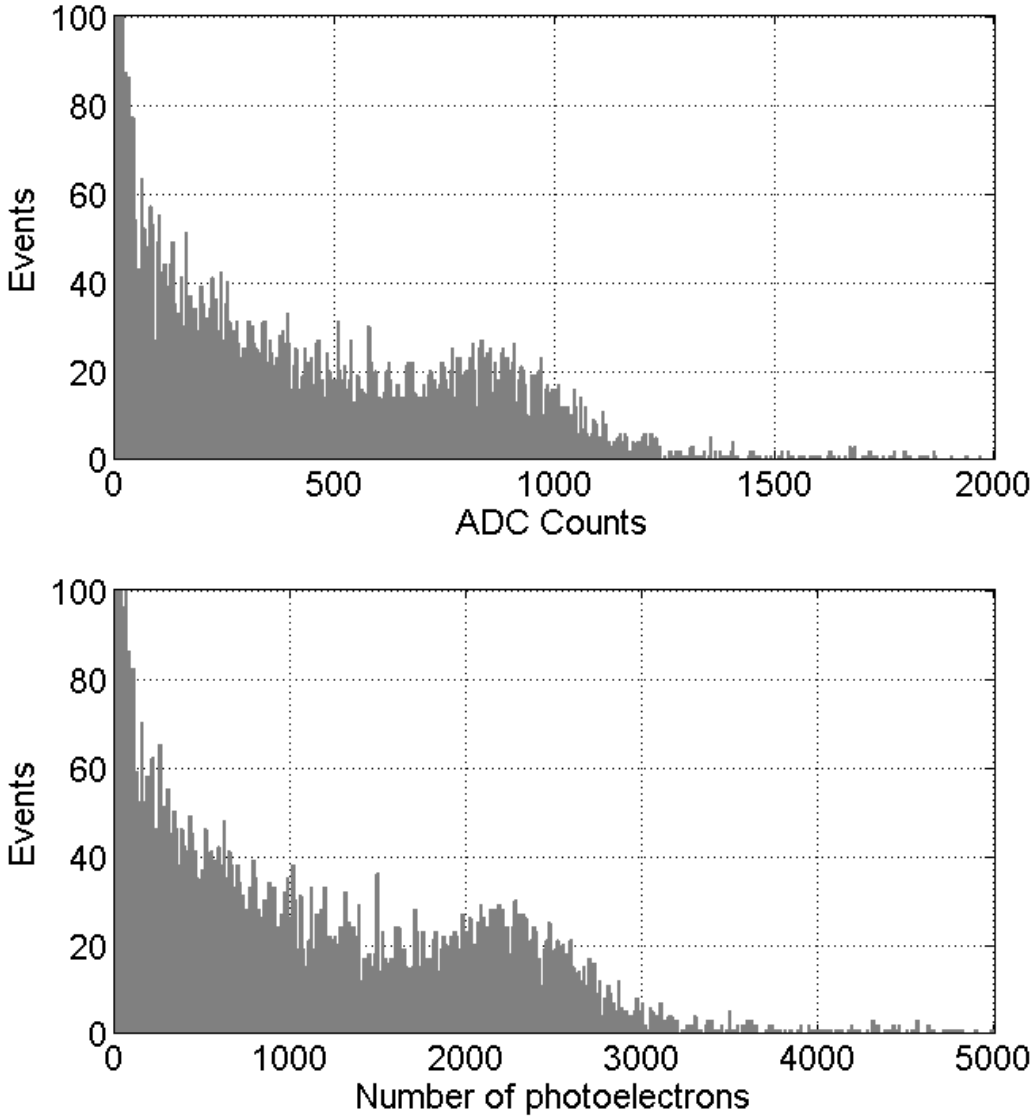

Figure 25: Muon spectrum in peak amplitude (top) and photoelectron (bottom) units.

4 Conclusions

The Neutrinos Angra target detector has recently been assembled with its 16 bottom PMTs. In order to equip the detector, the front-end and acquisition modules have been integrated with the purpose of assessing for the first time a full readout chain and the target detector of the experiment. This document presented in details the performed measurements needed to achieve the proposed goals, successfully validating the readout system and providing an indication, by means of the observed muon spectrum, of the proper operation of the target detector.

5 Acknowledgement

This work is supported by several agencies, through a number of funding projects. The Angra Collaboration acknowledges the support of Ministério da Ciência, Tecnologia e Inovação (MCTI), the Conselho Nacional para o Desenvolvimento Científico e Tecnológico (CNPq), Financiadora de Estudos e Projetos (FINEP) and the following state research agencies: FAPESP, FAPEMIG and FAPERJ. The collaboration also thanks the universities listed in the presentation page.

References

[1] José Abritta Costa, Eletrônica de Front-end do Experimento Neutrinos Angra, Master Thesis, Universidade Federal de Juiz de Fora, August 2014.

[2] Tony Igor Dornelas, Estudo, Desenvolvimento e Análise da Instrumentação do Experimento Neutrinos Angra, Master Thesis, Universidade Federal de Juiz de Fora, February 2015.

[3] Herman Lima Junior et al., Data Acquisition with Optimal Pulse Amplitude Estimation for a Neutrino Detection Experiment, Nota Técnica Vol. 4, N 2, p. 34-41, Centro Brasileiro de Pesquisas Físicas, 2014.

[4] Thamys Abrahão, Detecção de antineutrinos de reatores e medidas de fontes de ruído, Master Thesis, Centro Brasileiro de Pesquisas Físicas, 2012.